Electron distribution in MgO probed by x-ray emission

P. Jonnard, F. Vergand, and C. Bonnelle
Laboratoire de Chimie Physique Matière et Rayonnement, URA 176, Université Pierre et Marie Curie, 11 rue Pierre et Marie Curie, 75231 Paris Cedex 05, France

E. Orgaz and M. Gupta
Institut des Sciences des Matériaux, URA 446, Batiment 415, Université Paris-Sud, 91405 Orsay, France
(Received 22 December 1997)

The relative intensity of the Mg $K\beta$ emission band with respect to the $K\alpha$ atomic line, obtained by electron-induced x-ray emission spectroscopy, is used to investigate the variation of p-like valence electron number located around magnesium in metal and MgO. Calculated spectral intensities of Mg K emissions are obtained within the augmented plane-wave method for the perfect crystal. From experimental and theoretical data, the number of $3p$ electrons present around Mg and involved in the $K\beta$ transition does not vary much with the metallic or ionic character of the bonds. This result shows that the charge transfer is weak in the oxide. These experiments can be generalized to other compounds. Spectral densities of states (DOS) around Mg and O are also probed and agreement is found between experimental and theoretical spectral densities of $3p$ Mg and $2p$ O states. Changes of MgO valence DOS with annealing, etching, and aging are discussed. [S0163-1829(98)12419-0]

I. INTRODUCTION

Despite the large amount of data, the electronic distribution of alkaline-earth oxides is still controversial.[1,2] The determination of the mean number of electrons present around each element is of fundamental importance in relation to the redistribution of the electrostatic potential in the oxide and the degree of ionicity. These parameters depend on the atomic arrangement and on the presence of defects. They govern the physical and chemical properties such as electronic properties, structure, and reactivity of surfaces and metal-oxide interfaces.

An experimental approach is developed to investigate the electronic distribution of valence electrons in solid compounds. It involves the measurement of the relative *intensities* of x-ray emissions obtained by electron-induced x-ray emission spectroscopy (EXES).[3] The method is local and concerns thicknesses ranging from a superficial zone to the bulk, i.e., between 1 and 100 nm. By this method, the variation of the valence electron number, having a given symmetry, located around an element present in a metal or insulator, thin or bulk material can be probed. The *energy* distribution of local and partial densities of states (DOS) can be obtained simultaneously from the spectral density observed in the same sample. We have applied this method to the case of the magnesium present in the metal and the oxide.

A large number of theoretical investigations have been previously devoted to the study of the electronic properties of MgO and other alkaline-earth monoxides in relation to the possibility of a $B1$ to $B2$ structural transition under pressure.[4–8] Properties of the bulk material associated with various electronic transition spectra have been investigated,[9–12] as well as the energetics of intrinsic bulk-defect formation, vacancies as well as interstitials,[13–16] the electronic structure of surfaces,[17,18] and the molecule-surface interactions[19,20] found in catalysis. Indeed, MgO is considered the prototype for simple oxides. It is often treated as perfectly ionic. However, the presence of an interstitial charge should make the charge associated to each oxygen clearly inferior to 2.

Ab initio methods have been widely employed to investigate the bulk perfect crystal of MgO with sodium chloride structure. The most usual methods, augmented plane wave[8,16,21] (APW), Korringa-Kohn-Rostoker,[22,23] tight-binding,[4] pseudopotentials,[7,24] linear muffin-tin orbital,[25,26] linear augmented plane wave,[6,10] and linear combination of atomic orbitals[11,12] are based on the local-density approximation (LDA); the choice of different functionals[27–29] has also been examined. The general features of the band structure of bulk MgO are well established. Besides the empirical and Hartree-Fock[5,30] techniques, the direct energy gap is systematically underestimated by several eV, a common problem of all the LDA-based methods. Nevertheless, in the MgO case, the theoretical O p and Mg $s+p$ bandwidths are in reasonable agreement with spectroscopic data.

In the present work, we describe the experimental method and we compare the measured intensities to *ab initio* calculations of the spectral intensities. Only the distribution of the p-like electrons around the magnesium is studied experimentally. Agreement between experimental and theoretical data is satisfactory and proves the validity of the model used. Simultaneously, we observe $3p$ Mg and $2p$ O spectral densities; these densities agree with previous observations.[31–33] Comparison between our experimental and calculated partial spectral densities is presented. Samples of oxide having suffered various treatments are studied, and changes with the physicochemical characteristics of the sample are discussed.

In Secs. II and III, experimental techniques and results are reported. In Sec. IV, the computational method is presented. Theoretical results are discussed and compared to experimental data in Sec. V. This is made successively for the

TABLE I. Incident electron energy E_0 and analyzed thickness for each sample and each emission.

MgO sample	Emission line	E_0 (eV)	Analyzed thickness (Å)
Stored 2 months	O $K\alpha$	800	60
	Mg $K\beta$	3000	370
Cleaved	O $K\alpha$	800	60
		1500	200
		3000	500
	Mg $K\beta$	3000	370
Polished	O $K\alpha$	800	60
heated	Mg $K\beta$	300	370
etched	Mg $K\beta$	3000	370
etched heated	O $K\alpha$	650	35
		800	60
		1500	200
		3000	500
	Mg $K\beta$	1600	100
		2500	300
		3500	500
		4500	750
Film	Mg $K\beta$	4500	500

densities of states and for the electron distribution around the cation.

II. EXPERIMENTAL TECHNIQUES

A. EXES method

A core hole is created in a nlj subshell of an atom with atomic number Z by electron collision. This initial state relaxes by radiative transition to a final state with a less bound core or valence hole. The spectral density of the emitted photons is the convolution of the energy distributions of the initial and final states, multiplied by the transition probability. The intensity of the x-ray emission depends on the number of the initial states, the radiative transition probability, and the self-absorption of the emitted radiation.[3]

The analyzed thickness is determined by means of an semiempirical model,[34,35] which takes into account the energy and angular distributions of incident and backscattered electrons, the electron ionization cross sections, and the absorption of the emitted photons. For the incident electron energy E_0, we determine the ratio $P(x)=I(x)/I(\infty)$ where $I(x)$ is the intensity emitted from a thickness x of the sample, and $I(\infty)$ the intensity from an infinite thickness. For single crystals, we consider that the relevant value of the analyzed thickness is that corresponding to $P(x)=0.80$. For thin films the whole thickness is analyzed. The incident electron energies E_0 are reported in Table I together with the ''analyzed thickness'' for each emission and each sample.

1. Spectral density of valence states

When the final hole is present in the valence band, the spectral density of the emitted photons describes the distribution of the final state broadened by the energy distribution of the initial state, which is a Lorentzian curve of known width, and multiplied by the square of the matrix element. If the matrix element is assimilated to a constant along the emission band, the spectral density probes the valence DOS. Because of the transition matrix element, x-ray emission gives information on the local (given Z) and partial (given symmetry $s,p,d,\ldots$) DOS. The local character is due to the spatial localization of the core hole and the partial character due to the dipole selection rules.

2. Charge distribution

The probability of x-ray atomic emissions, i.e., emissions between normally filled subshells, can be considered, in first approximation, as independent of the physicochemical state of the Z element. By contrast, the probability of emission from the valence band is a function of the valence electron number of $l\pm1$ symmetry present in the vicinity of the core hole. Then a change of the valence electron distribution can be deduced from a change of the relative intensity of the valence-band emission, measured with respect to the intensity of an atomic emission having the same initial state. For the $10<Z<18$ elements, by considering the $K\beta$ ($3p$-$1s$) and $K\alpha$ ($2p$-$1s$) lines and making the approximation that the probability of the $K\alpha$ line does not depend on the physicochemical state, it is possible to determine the $3p$ electron mean number present around the Z element, from the measurement of the intensity ratio $R=K\beta/K\alpha$. A change of the s distributions can be observed for $Z>18$. Indeed, s distributions are deduced from transitions to p holes and no atomic line to $2p$ exists for the $Z<18$ elements. Similarly, no atomic line to $1s$ exists for oxygen.

We have measured the intensity of Mg $K\beta$ with respect to that of Mg $K\alpha$ by using the same ionization conditions for both emissions. The number of initial states is thus the same for $K\alpha$ and $K\beta$ and the intensity ratio $R=K\beta/K\alpha$ does not depend on this number. We have chosen experimental conditions such that the self-absorption of the radiation in the target is weak. In this case, the ratio of the self-absorption terms can be approximated to unity. Then the ratio R is equal to the ratio of the $K\beta$ and $K\alpha$ radiative probabilities. By making the approximation that the probability of $K\alpha$ does not depend on the material, we have deduced from the value of R the variation of the $3p$-$1s$ matrix element, i.e., the variation of the Mg $3p$ electron number, present near the Mg $1s$ inner hole, between the metal and the oxide.

3. Experimental conditions

X-ray spectra were obtained with the aid of a bent-crystal x-ray vacuum spectrometer of the Johann type that gives a spectral resolution of 10^{-4}.[36] The bent crystals, 500 mm radius, were (100) TlAP and (1010) beryl blades with planes parallel to the curved faces. The detector was a gas flow counter (90% Ar–10% CH_4) working in the Geiger region. The incident electron beam made a 10° angle with respect to the normal of the sample. During the analysis the sample was under ultrahigh vacuum. The sample temperature can be var-

ied between 120 and 550 K and kept constant to within ± 1 K below 260 K and ± 5 K above 260 K.[37]

The O $K\alpha$ emission was recorded for $h\nu$ between 518 and 530 eV, the Mg $K\beta$ one between 1287 and 1310 eV in order to investigate both the upper valence band (up to ~ 1300 eV) and states in the band gap. The spectral densities of O $2p$ and Mg $3p$ valence states, respectively, are obtained from these emissions. The broadening of the valence-band edges in O $K\alpha$ and Mg $K\beta$ is evaluated by making the sum of calculated instrumental and intrinsic widths. They are 0.5 and 0.9 eV, respectively. Oxygen $K\alpha$ emission was observed at high and low incident electron energy with the aim of comparing the spectral densities in the bulk and in a superficial zone of the sample. For Mg $3p$, experimentation at high incident electron energy only was made because the intensity of the Mg $K\beta$ emission is weak.

The magnesium $K\alpha$ is situated at 1253.5 eV; it is made up of two Lorentzian lines, $K\alpha_1$ and $K\alpha_2$ separated by the $2p$ spin-orbit coupling of 0.28 eV.[38] The intensity ratio Mg $K\alpha_1$/Mg $K\alpha_2$ is about 2. The experimental width at half-maximum of $K\alpha_1$ and $K\alpha_2$ is 1.2 ± 0.1 eV. This value agrees with that obtained by adding the intrinsic broadening, due to the lifetime of the $1s$ hole (we neglect the broadening due to the lifetime of the $2p$ hole), and the calculated instrumental broadenings due to the crystal dimensions.

B. Samples

The samples are air cleaved (100) single-crystal blades and were obtained using various treatments, and thin films were deposited by thermal evaporation of similar crystals. Quantitative analysis of the single crystals was performed by neutronic activation at Laboratoire ''Pierre Süe'' in CEA-Saclay. The main impurity is Ca with concentration lower than 0.08 wt %. Other impurities, Fe, Cr, and Mn, are less than 0.01 wt %. From images of air-cleaved single crystals, obtained by means of transmission electron microscopy and high-energy electron diffraction patterns, wide flat areas and zones with high density of dislocations are present but retain the normal interatomic distance. From electron diffraction patterns, thin films are polycrystalline.

Air-cleaved (100) single crystals stored under air during long (2 months) and short (1 h) times were compared. One same crystal was polished and annealed at 1270 K under air during 25 h. Others were cleaned *in situ* by means of (i) heating at 770 K during 1 h; (ii) Ar^+ 2 keV etching; (iii) alternating etching and heating at 620 K during 6 h. The effect of *in situ* argon ion etchings, 0.5 and 2 keV, on the crystal polished and annealed under air was also examined. A 500-Å-thick polycrystalline film was deposited by electron bombardment on a NaCl substrate coated by a 400-Å Cu film.

III. EXPERIMENTAL RESULTS

Spectra are recorded in a photon energy scale. The background is subtracted and the curves are normalized with respect to the maximum amplitude. The binding-energy scale relative to the top of the valence band E_v is also plotted as an upper line on the graphs. The energy E_v is obtained by adjusting the main peak of Mg $3s$ and O $2p$ spectral densities with that of the corresponding partial calculated DOS. For Mg $3p$ spectral density, E_v is determined by fitting the valence-band edge by a linear law $(E-E_v)$ convoluted with a 0.9-eV-wide Lorentzian curve.

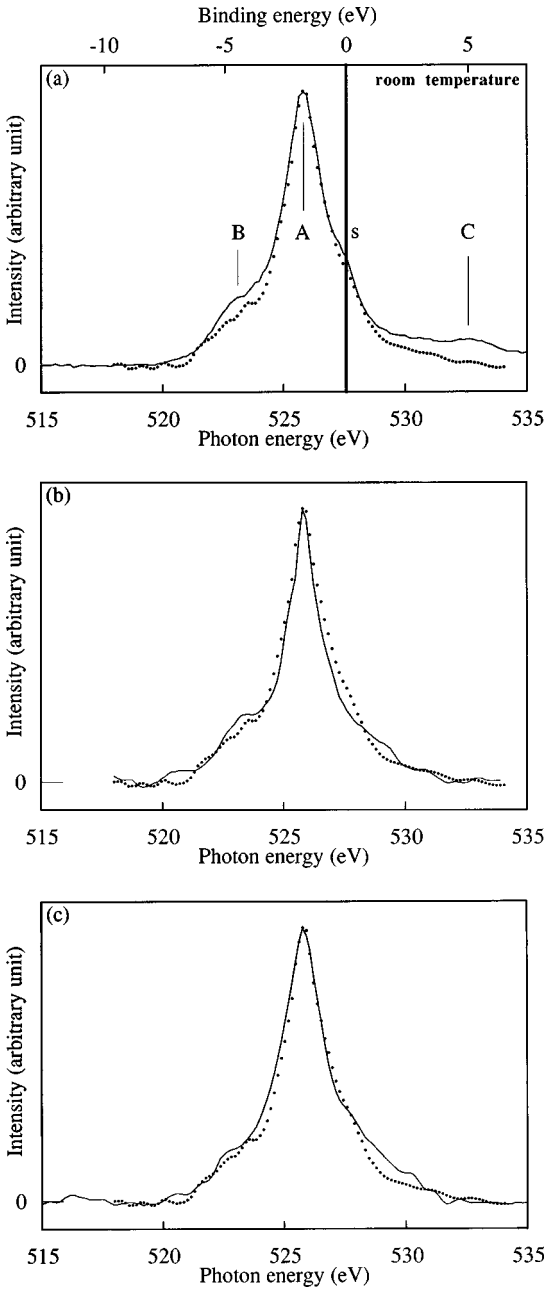

FIG. 1. O $2p$ spectral densities of MgO: (a) solid line, bulk; dots, superficial zone. (b) Superficial zones: solid line, at 530 K; dots, at 330 K. (c) Superficial zones: solid line, after Ar etching; dots, before etching.

A. Oxygen $2p$ spectral density

The oxygen $2p$ spectral density of a cleaved MgO single crystal, obtained at $E_0 = 3000$ eV at room temperature, is plotted in Fig. 1(a) (solid line). A main peak (A) is observed at $h\nu = 525.7 \pm 0.1$ eV and a structure (B) appears on the low photon energy side. The shoulder s on the high photon en-

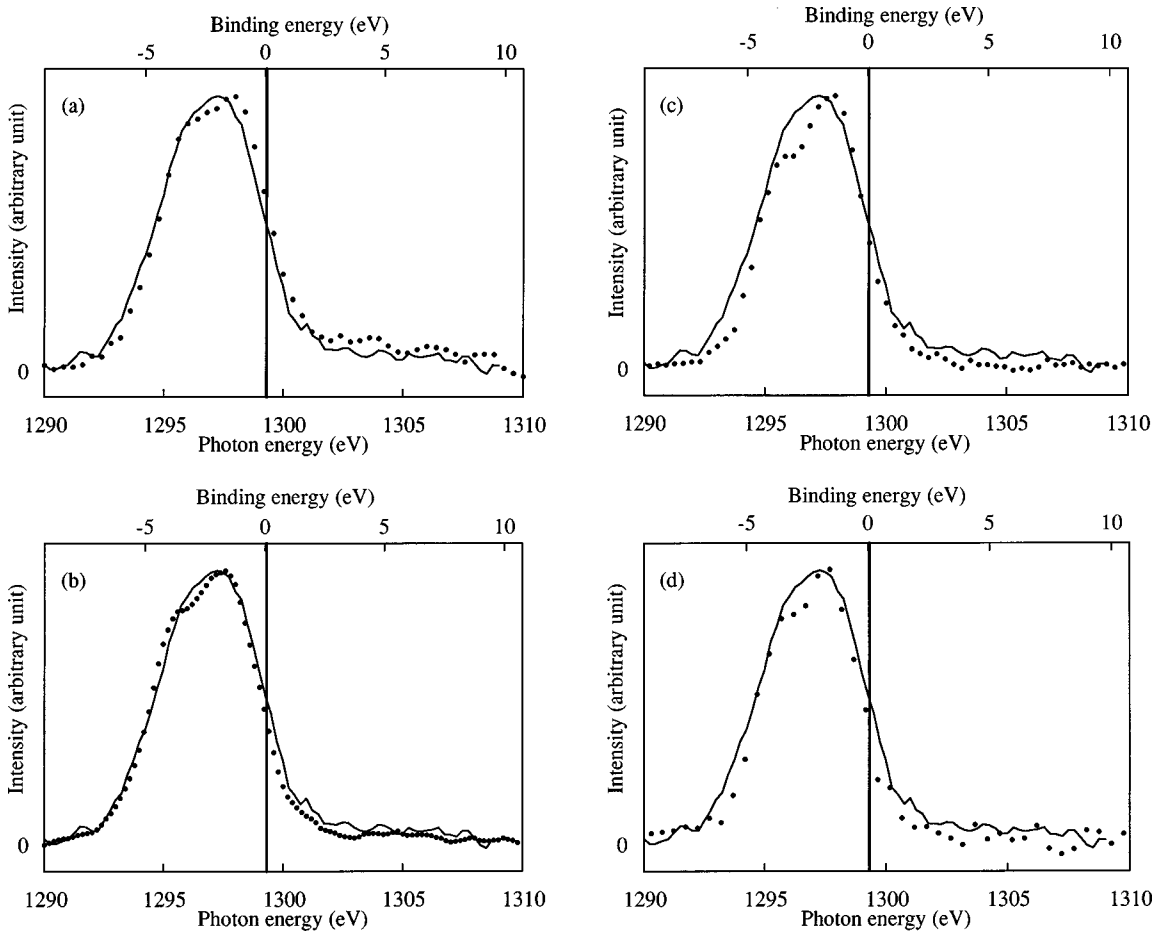

FIG. 2. Mg $3p$ spectral densities of MgO. Solid line, reference sample, compared to dots. (a) Cleaved stored 2 months sample; (b) heated in UHV sample; (c) Ar-etched sample; (d) film sample.

ergy side is a satellite emission.[33] The structure C observed at higher photon energies is due to the anomalous reflection from the crystal analyzer. The binding energies $E-E_v$ are 1.0 ± 0.1 eV for peak (A) and about 3.7 eV for structure (B), giving 2.7 eV for the A-B distance. The spectral density does not depend on the temperature of the sample and on the *in situ* treatments for incident energies E_0 clearly above the O $1s$ ionization threshold.

Changes in the O $2p$ density are observed when E_0 is decreased below about 800 eV, i.e., when the analysis concerns a superficial zone of the sample. First, at 650 eV and at room temperature, the intensity of structure (B) decreases [Fig. 1(a), dots]. Second, the satellite s is not observed because the incident energy is not sufficient to excite it. The decreasing of (B) and s intensities induces a slight narrowing of the main peak. A comparison of the spectral densities at 650 eV and at two temperatures, 300 and 500 K, is presented in Fig. 1(b). At high temperature, a marked narrowing of the main peak appears, mainly towards the lower binding energies, whereas the intensity of structure (B) is approximately the same as in the volume analysis. No energy shift of peak (A) is seen. Changes are also observed at room temperature for the etched sample whose main peak is spread more towards lower and higher binding energies than for the freshly cleaved sample [Fig. 1(c), solid line].

B. Magnesium $3p$ spectral density

The magnesium $3p$ spectral density of the bulk varies according to the treatments given to the sample and depends slightly on the temperature. All the curves presented are obtained at room temperature. We refer our results to the spectral density obtained for the polished (100) single crystal annealed under air at 1000 °C [solid line of Figs. 2(a)–2(d)]. This density presents a main peak situated at $h\nu=1297.2\pm0.1$ eV (binding energy $E-E_v=2.9\pm0.1$ eV). A badly resolved secondary peak is located at $E-E_v=4$ eV. Analogous spectral density is obtained for the freshly cleaved crystal.

The dots in Fig. 2(a) describe the spectral density of the MgO crystal stored during 2 months after cleaving. The main peak is shifted by 0.8 eV towards lower binding energies and this shift is accompanied by a broadening in the same energy range. This suggests that the emission has supplementary components, due to chemical bonds of Mg with contaminants, carbonates, or hydroxyl groups. This spectral density is characteristic of a contaminated sample.

The dots in Fig. 2(b) correspond to the spectral density of the UHV annealed crystal. This density is similar to that of the reference sample towards the lower binding energies. It is weaker in the range of the secondary maximum. Analogous effect but clearly more marked is seen for the UHV etched

sample; indeed the structure at 4 eV is the weakest for this sample. This decrease is accompanied by a narrowing in the range of higher binding energies and also at the low part of the peak towards the lower binding energies [Fig. 2(c), dots]. The spectral density of the MgO film is presented in Fig. 2(d) (dots). It is rather similar to that observed for the etched sample. Changes with increasing temperature and annealing are also seen in the range of the secondary maximum. In this range, the intensity is the highest for the sample taken as reference.

In the energy range of the optical gap, the larger intensity is emitted by the sample stored 2 months [Fig. 2(a)] and the weaker by the UHV etched sample [Fig. 2(c)]. For the other samples, the intensity is weak and approximately equivalent (Fig. 2).

C. Intensity ratio of Mg $K\beta$ and $K\alpha$ emissions

The intensity ratio R of Mg $K\beta$ and $K\alpha$ emissions was determined for each sample. A large number of measurements were made by varying the temperature between 120 and 550 K and the incident energy E_0 between 1.6 and 4.5 keV. As already underlined, the analyzed thicknesses depend on E_0 (cf. Table I). No variation of R was observed with the temperature and with E_0 between 2.5 and 4.5 keV. In this energy range, the analyzed thicknesses make the results characteristic of the bulk. The mean value of R is 0.021 ± 0.002. A value of 0.019 was obtained for the reference sample. On the other hand, a lower value of 0.018 was observed for $E_0 = 1.6$ keV, i.e., for the superficial zone; this decrease is characteristic of changes of the atomic arrangement in this zone.

IV. COMPUTATIONAL METHOD

The APW method[39] was used to calculate *ab initio* the energy bands of MgO at 89 **k** points in the irreducible wedge of the fcc Brillouin zone (BZ) and at 364 **k** points in the irreducible wedge of the hexagonal BZ for metallic magnesium. The crystal potential was treated within the muffin-tin (MT) approximation with warped muffin-tin correction in the external region outside the MT spheres. The LDA was used to determine the exchange term of the crystal potential within the approach of von Barth and Hedin.[28]

The energy cutoff was fixed in order to ensure a 1-mRy convergence in the eigenvalues. The total DOS and its partial wave analysis, into its s, p, and d components, inside the MT sphere was calculated by means of the accurate linear energy tetrahedron integration scheme.[40]

The x-ray emission intensity $I(E)$ is given in the one-electron approximation by

$$I(E) = C \sum_n \int d^3k |\langle \psi_c | \mathbf{r} | \psi_{\mathbf{k},n} \rangle|^2 \delta(E - E_{\mathbf{k},n} + E_c), \quad (1)$$

where $\psi_{\mathbf{k},n}$ and $E_{\mathbf{k},n}$ are, respectively, the Bloch function and Bloch energy of an electron in the valence band with wave vector $\mathbf{k}$ and band index n, ψ_c is the core wave function ($1s$ function for Mg K spectrum) with energy E_c. The integral in Eq. (1) is performed over constant energy surfaces $E = E_{\mathbf{k},n} \pm E_c$. If the transition matrix elements $\langle \psi_c | r | \psi_{\mathbf{k},n} \rangle$ are taken as constants, the K emission is proportional to the p component of the DOS.

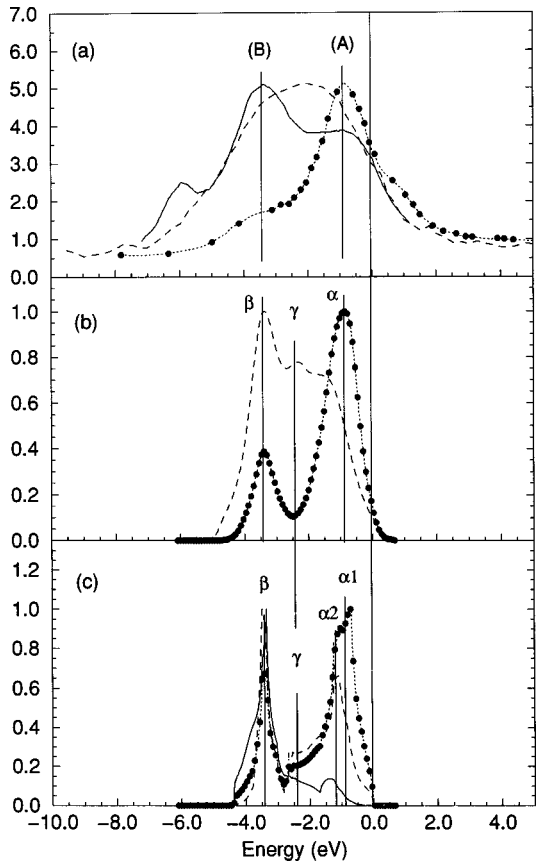

FIG. 3. MgO (a) experimental spectral densities: solid line, Mg $3s$ (the feature around -6 eV is due to the $2p$-$2s$ atomic line); dashed line, Mg $3p$; dotted line, O $2p$. (b) Calculated spectral densities: dashed line, Mg $3p$; dotted line, O $2p$. (c) Calculated DOS: solid line, Mg $3s$; dashed line, Mg $3p$; dotted line, O $2p$.

The matrix elements of the transition probabilities between the valence-band states and the $1s$ final core state of Mg and O, respectively, were calculated using the dipolar length form. A strong **k** dependence of these matrix elements was observed. However, after performing the reciprocal space integration, these matrix elements are found to depend only weakly on the energy. The convergence of the calculation was obtained with 6656 microtetrahedra in the irreducible wedge of the fcc BZ; increasing the number of tetrahedra to 53 248 did not result in any significant change in the calculated values.

V. THEORETICAL RESULTS AND COMPARISON WITH EXPERIMENT

A. Spectral densities of states

We present in Fig. 3 the O $2p$ and Mg $3p$ spectral densities of the reference sample compared to the Mg $3s$ spectral density[41] [Fig. 3(a)], and to the calculated partial [Fig. 3(c)] and spectral DOS's [Fig. 3(b)]. All curves are normal-

ized with respect to the maximum and are referred to the energy of the top of the valence band E_v.

The features of the band structures and DOS obtained for MgO and Mg are in general agreement with previous calculations performed with similar methods.[6–8,42] The total valence band of MgO extends over two clearly spaced energy regions. The lower energy part corresponds to O $2s$ states mixed with Mg states. Only the higher energy part, of width 4.5 eV, is plotted here. It is dominated by the contribution of the O $2p$ states. The partial wave DOS analysis inside the magnesium MT sphere of radius $R_{\mathrm{Mg}} \approx 1.65$ a.u., shown in Fig. 3(b), indicates the presence of Mg s and Mg p states in this energy range. Their respective contributions correspond to 0.050 and 0.078 electrons. The corresponding DOS presents two main peaks centered, respectively, at 1 and 3.5 eV below the top of the valence band.

In the partial DOS's O p, Mg s and p, plotted in Fig. 3(c), four structures labeled (α_1), (α_2), (γ), and (β) are present. The top of the band (α_1) corresponds mainly to a peak in the O $2p$ states. Just below, an overlap exists between O $2p$ and Mg states. Indeed, the (α_2) structure corresponds to a coincidence between O $2p$, Mg $3p$, and Mg $3s$ states. Structures are present in Mg $3s$ and $3p$ DOS in coincidence with the structure (γ) and a narrow peak appears in the three partial DOS's at the position of the peak (β). In Fig. 3(b), the O $2p$ and Mg $3p$ spectral densities calculated by means of Eq. (1) have been convoluted by Lorentzians of full width at half maximum 0.5 and 0.9 eV, respectively, to take into account the intrinsic width due to the core hole lifetime and the instrumental resolution. The structures (α) and (β), separated by 2.6 eV in the calculated spectral densities, correspond, respectively, to the observed (A) and (B) structures in the experimental spectra. From a comparison of the partial DOS's [Fig. 3(c)] and the calculated spectra [Fig. 3(b)], it appears that the energy dependence of the matrix elements leads to a decrease in the intensity of structure (β) relative to (α_1) in the O $2p$ spectral density. This trend is in agreement with the experimental observation. In the calculated Mg $3p$ spectral density of MgO, the transition matrix elements lower the intensity of the (α_2) structure relative to that of the (β) structure. By contrast, the peak (A) is higher than the structure (B), as seen from the Mg $3p$ spectral densities plotted in Fig. 2. The difference between experimental and calculated DOS is the smallest for the reference sample. The role of the transition probabilities suggests that pure Mg p-like states should be present in the B region while from the experiment Mg p spectral DOS is weak in this range.

1. Changes of the O 2p states

No change of the O $2p$ spectral density is seen for the bulk, whatever the treatments given to the sample. On the other hand, for the superficial zone of heated or etched sample, the spectral density is modified (Fig. 1). The changes concern the relative intensity of the structure B, that is to say, the O $2p$ states that are more strongly mixed with the Mg states. This structure is weaker in the superficial zone than in the bulk, indicating a decrease in the mixing of O and Mg states around the oxygen and, consequently, a decreasing of the ionicity: this is due to the presence of the surface and of defects.

The spectral density of the superficial zone is sensitive to the treatment and to the temperature. As an example, the density of states of the etched sample is enlarged and a structure is seen in the range of the optical gap. These results can be explained by the presence of defects, whose states are expected in this energy range. The narrowing of the spectral density towards the low binding energy, observed with increasing temperature, suggests an improvement of the surface quality.

2. Changes of the Mg 3p states

Mg $3p$ spectral density is more sensitive to the physicochemical state of the sample than the O $2p$ one. Indeed, changes are seen for the bulk. Except for the contamined sample, the main changes are present in the 3–5 eV range. They correspond to a variation in the relative intensities of the (A) and (B) peaks. The relative importance of structure (B) is maximum for the reference sample and the lower for the etched sample. The decrease of structure (B) reveals a larger hybridization between the Mg $3p$ and O $2p$ states around the magnesium, thus a decrease of the ionic character. Thus we expect that the ionicity is the largest for the reference sample. Let us note that the etching introduces defects in a superficial zone. Thus the presence of defects decreases the ionicity of MgO.

We have calculated the Mg $3p$ spectral density of metallic Mg; it is plotted in Fig. 4 together with the partial wave analysis of the DOS. Besides its expected parabolic shape, the conduction band of Mg of total width 6.1 eV presents a peak centered around 1.1 eV below the Fermi level that is due to Mg p states. While the s states contribution dominates at low energy, the Mg p and d characters increase with increasing energy. At E_F, the major contribution is provided by the Mg p states. The transition matrix elements lead to a relative increase of the intensity of the p states close to the Fermi level. The Mg $3p$ spectral density of metallic Mg convoluted by a Lorentzian of 0.9 eV width presents a peak around 1 eV below the Fermi level. Its shape is very different from that calculated in the oxide in agreement with the experimental observation [Fig. 4(a)].

B. Electronic distribution

The presence of Mg $3p$ states around the Mg ion reveals the partially ionic character of bonds in MgO and a decrease of the ratio R is characteristic of a increase of the ionic character. As seen in the previous section, the Mg $3p$ states are sensitive to changes of the Mg environment. The same is true for the ratio R. Thus, for the reference sample, R is relatively small, in agreement with the increasing ionic character predicted from the shape of the Mg $3p$ spectral density.

With the aim to determine the contribution of $3p$ states in the oxide with respect to the metal, we have determined the value of R for metallic Mg. We obtain a value of 0.018, smaller than that observed for the oxide.

An analysis of the Mg $3p$ change inside magnesium MT spheres of radii $R_{\mathrm{Mg}} = 1.65$ a.u. has been performed. The partial wave decomposition of the DOS indicates an increase in the number of Mg p electrons from 0.0604 in metallic Mg to 0.0780 in MgO. This trend is slightly further enhanced by

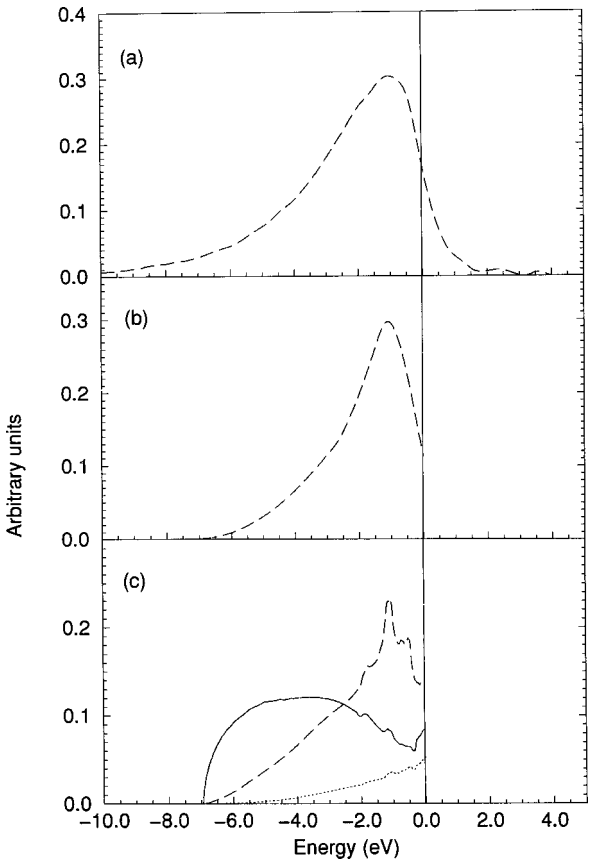

FIG. 4. Mg metal, (a) experimental spectral densities of $3p$ states, (b) calculated spectral densities of $3p$ states, (c) calculated DOS: solid line, s states; dashed line, p states; dotted line, d states.

the transition matrix elements since the calculated $3p$ spectral density corresponds to 0.0399 and 0.055 electrons, respectively, for metallic Mg and MgO. Thus the calculated ratio $K\beta$ MgO/$K\beta$ Mg amounts to 1.37 (with matrix elements included) and to 1.29 without matrix elements. The theoretical results fall in the experimental range that is estimated to 1.2 ± 0.1.

We want to emphasize at this point that the Mg sphere radius used for the calculations in MgO is relevant to the present discussion of the Mg K spectrum because the $1s$ core function is entirely localized in a sphere of such radius. In contrast, the number of delocalized valence electrons of s and p character is small in such a sphere.

We find that the number of s electrons decreases drastically from 0.092 in metallic Mg to 0.050 in MgO as one would expect in an ionic compound. However, the increase, although modest, in the number of p electrons from Mg to MgO obtained in the experimental data as well as in the calculations deserves further analysis since it is not expected from simple arguments of ionicity.

Since the crystal structure and Mg-Mg distances in metallic hexagonal Mg and in NaCl structure MgO are different, we have performed a calculation in which we replaced the oxygen spheres of MgO by empty spheres. The charge analysis inside the magnesium MT sphere leads to 0.098 s electrons and 0.079 p electrons. We thus obtained a number of p electrons marginally higher than in MgO. This shows that between magnesium and oxygen, if we consider the p electrons contained only in the magnesium MT sphere, the flow of charge is almost nil. The small increase in the number of p electrons relevant to the Mg K spectrum between hexagonal Mg and MgO results only from the differences in interatomic distances.

At this point we wish to point out that in MgO, inside the oxygen MT sphere having the radius R_W of a Watson sphere,[43] the self-consistent APW integrated charge is about 8.9 while it is about 10 in the Mg sphere and 1.1 in the interstitial region. Superposition of the charge densities of the neutral atoms gives already 8.5 electrons inside the O sphere. Thus, a large amount of the charge around the O site is due to charge superposition, besides charge transfer. This feature of the charge distribution in ionic crystals has been already discussed by Slater.[44] Then, the value of the integrated charge should be taken with caution for analysis in terms of ionicity.[21]

VI. CONCLUSION

As it is well known, it is possible to deduce by EXES information on the energy distributions of the valence states. We have analyzed by this method the O $2p$ and Mg $3p$ DOS in monocrystalline MgO in relation with the characteristics of the sample. Changes of the valence DOS have been seen with annealing, etching, and aging. These treatments modify the stoichiometry, introduce defects, and thus change the atomic environment in the oxide. On the other hand, drastic differences are observed between metallic Mg and Mg in the oxide,[31] in general agreement with the calculated spectra. Then, in spite of the low number of Mg $3p$ electrons present at the vicinity of the core, the Mg $3p$ spectral density is a very sensitive probe of the valence distributions.

We suggest that information can be obtained by EXES on the electronic distributions around an element present in a material. This is possible by measuring the intensity of the emission band with respect to that of a convenient atomic emission. Using this method, we have shown that the $3p$ electron number around the magnesium is practically the same in the metal and MgO. This result is in agreement with the spectral intensities calculated in this work. On the other hand, we have observed changes of the Mg $3p$ electronic distribution between the bulk sample and a superficial zone at the surface and also between bulk samples having undergone treatments under air or ultravacuum. Then variation of the electronic charge around Mg can be observed as a function of the atomic environment. The experimental method proposed in the present paper can be extended to the $Z > 10$ elements present in any material.

ACKNOWLEDGMENTS

The authors wish to thank Professor E. Gillet and Dr. M. Backhaus-Ricoult for providing some samples and Dr. G. Revel for neutronic activation analysis. They acknowledge IDRIS, Centre National de la Recherche Scientifique, for the use of its computer facilities. Part of this work was done within the framework of the Groupe de Recherche 1108.

[1] G. Pacchioni, C. Sousa, F. Illas, F. Parmigiani, and P. S. Bagus, Phys. Rev. B **48**, 11 573 (1993).
[2] R. Souda, K. Yamamoto, W. Hayami, T. Aizawa, and Y. Ishizawa, Phys. Rev. B **50**, 4733 (1994).
[3] C. Bonnelle, *Annual Report C 1987* (Royal Society of Chemistry, London, 1987), pp. 201–272.
[4] G. Kalpana, B. Palanivel, and M. Rajagopalan, Phys. Rev. B **52**, 4 (1995).
[5] E. Apra, M. Causa, M. Prencipe, R. Dovesi, and V. R. Saunders, J. Phys.: Condens. Matter **5**, 2969 (1993).
[6] M. J. Mehl, R. E. Cohen, and H. Krakauer, J. Geophys. Res. **93**, 8009 (1988).
[7] K. J. Chang and M. L. Cohen, Phys. Rev. B **30**, 4774 (1984).
[8] M. S. T. Bukowinski, J. Geophys. Res. **85**, 285 (1980).
[9] M. Grass, J. Braun, and G. Borstel, Surf. Sci. **331-333**, 1526 (1995).
[10] V. S. Stepanyuk, A. Szasz, A. A. Grigorenko, A. A. Katsnelson, O. V. Farberovich, V. V. Mikhalin, and A. Henry, Phys. Status Solidi B **173**, 633 (1992).
[11] Y.-N. Xu and W. Y. Ching, Phys. Rev. B **43**, 4461 (1991).
[12] P. F. Walch and D. E. Ellis, Phys. Rev. B **8**, 5920 (1973).
[13] L. N. Kantorovich, J. M. Holender, and M. J. Gillan, Surf. Sci. **343**, 221 (1995).
[14] A. M. Ferrari and G. Pacchioni, J. Phys. Chem. **99**, 17 010 (1995).
[15] A. de Vita, M. J. Gillan, J. S. Lin, M. C. Payne, I. Stich, and L. J. Clarke, Phys. Rev. Lett. **68**, 3319 (1992); Phys. Rev. B **46**, 12 964 (1992).
[16] B. M. Klein, W. E. Pickett, L. L. Boyer, and R. Zeller, Phys. Rev. B **35**, 5802 (1987).
[17] E. Castanier and C. Noguera, Surf. Sci. **364**, 1 (1996); **364**, 17 (1996).
[18] A. Gibson, R. Haydock, and J. P. LaFemina, Phys. Rev. B **46**, 12 964 (1992).
[19] S. Russo and C. Noguera, Surf. Sci. **251/252**, 1081 (1992).
[20] C. Noguera, J. Goniakowski, and S. Bouette-Russo, Surf. Sci. **287/288**, 188 (1993).
[21] J. Redinger and K. Schwarz, Z. Phys. B **40**, 269 (1981).
[22] T. Kotani and H. Akai, Phys. Rev. B **54**, 16 502 (1996).
[23] J. Yamashita and S. Asano, J. Phys. Soc. Jpn. **28**, 1143 (1970).
[24] E. V. Zarochentsev, E. P. Troitskaya, and E. Y. Fain, Fiz. Tverd. Tela (Leningrad) **21**, 438 (1979) [Sov. Phys. Solid State **21**, 259 (1979)].
[25] U. Schönberger and F. Aryasetiawan, Phys. Rev. B **52**, 8788 (1995).
[26] O. E. Taurian, M. Springborg, and N. E. Christensen, Solid State Commun. **55**, 351 (1985).
[27] J. C. Slater, Phys. Rev. **81**, 385 (1951).
[28] U. von Barth and L. Hedin, J. Phys. C **5**, 1629 (1972).
[29] L. Hedin and B. I. Lundqvist, J. Phys. C **4**, 2064 (1971).
[30] R. Dovesi, C. Roetti, C. Freyria-Faya, E. Apra, V. R. Saunders, and N. M. Harrison, Philos. Trans. R. Soc. London, Ser. A **341**, 203 (1992).
[31] C. Sénémaud, J. Phys. (France) **32**, 89 (1971).
[32] M. Linkaoho, J. Utriainen, and J. Valjakka, Solid State Commun. **19**, 399 (1976).
[33] K. Maeda, M. Uda, and Y. Hayasi, Phys. Lett. **112A**, 431 (1985).
[34] P.-F. Staub, X-Ray Spectrom. **27**, 43 (1998).
[35] P.-F. Staub, P. Jonnard, F. Vergand, and C. Bonnelle, X-Ray Spectrom. **27**, 58 (1998).
[36] C. Bonnelle, F. Vergand, P. Jonnard, J.-M. André, P.-F. Staub, P. Avila, P. Chargelègue, M.-F. Fontaine, D. Laporte, P. Paquier, A. Ringuenet, and B. Rodriguez, Rev. Sci. Instrum. **65**, 3466 (1994).
[37] P. Jonnard, P. Chargelègue, C. Hombourger, J. Thirion, and F. Vergand, Rev. Sci. Instrum. **67**, 2417 (1996).
[38] P. H. Citrin, G. K. Wertheim, and Y. Baer, Phys. Rev. B **16**, 4256 (1977).
[39] L. C. Mattheiss, J. H. Wood, and A. C. Switendick, in *Methods in Computational Physics 8*, edited by B. Adler, S. Fernbach, and M. Rotenberg (Academic, New York, 1968).
[40] G. Lehmann and M. Taut, Phys. Status Solidi B **54**, 469 (1972).
[41] W. L. O'Brien, J. Jia, Q.-Y. Dong, T. A. Callcott, D. R. Mueller, D. L. Ederer, and C.-C. Kao, Phys. Rev. B **47**, 15 482 (1993).
[42] R. P. Gupta and A. J. Freeman, Phys. Rev. Lett. **36**, 1194 (1976).
[43] R. E. Watson, Phys. Rev. **111**, 1108 (1958).
[44] J. C. Slater, *Symmetry and Energy Bands in Crystals* (McGraw-Hill, New York, 1965), Vol. 2.